East European Journal of Physics. **3**. 127–137 (2026)

DOI: 10.26565/2312-4334-2026-3-11 ISSN 2312-4334

TRAVERSABLE WORMHOLE SOLUTIONS THROUGH DECOUPLING APPROACH IN RASTALL THEORY

Muhammad Sharif[1,2*], **Malick Sallah**[1], **Tayyab Naseer**[1*]

[1]*Department of Mathematics and Statistics, The University of Lahore, 1-KM Defence Road Lahore-54000, Pakistan*

[2]*Jadara Research Center, Jadara University, Irbid 21110, Jordan*

[*]*Corresponding Author e-mail: msharif.math@pu.edu.pk; tayyabnaseer48@yahoo.com*

Received May 17, 2026; revised August 11, 2026; accepted August 17, 2026

This paper explores the construction of traversable wormhole solutions in the context of Rastall's gravity using the extended gravitational decoupling method. Based on the modified field equations of this new theory, we apply the present scheme to incorporate an extra gravitational source, which leads to a fully transformed version of the Schwarzschild solution. By means of an appropriate coordinate transformation, this modified geometry is reinterpreted as a wormhole spacetime. The analysis proceeds by investigating the resulting configuration's fundamental physical and geometric features, specifically, null energy conditions' violation, gravitational mass behavior, volume integral quantifier evaluation, and embedding diagram. A key finding is that the wormhole neck arises obviously from the distorted geometry while also satisfying the traversability-required flare-out criterion. Plotting the energy conditions for various Rastall parameter values reveal localized null energy condition violations near the throat, which is consistent with the presence of exotic matter. However, the total exotic matter content is shown to be minimal and highly sensitive to the choice of model parameters. These results underscore the potential of Rastall gravity, in conjunction with gravitational decoupling, to support physically plausible wormhole geometries with reduced exotic matter requirements.

Keywords: *Rastall theory; Gravitational decoupling; Wormholes; Exotic fluid*

1. INTRODUCTION

In recent years, modified gravity frameworks have garnered considerable attention as viable alternatives to general relativity (GR), especially in addressing challenges related to dark energy, cosmic expansion, and spacetime singularities. Among the most prominent approaches are $f(\mathcal{R})$ gravity and scalar-tensor formulations, both of which have been extensively studied for their potential to offer deeper insights into gravitational dynamics [1, 2]. Within this broader investigative landscape, the Rastall theory [3] stands out by deviating from the standard conservation of the energy-momentum tensor (EMT) in curved geometries. By introducing a coupling between the EMT divergence and the gradient of the Ricci scalar, Rastall's model proposes a non-minimal interaction between matter and geometry, suggesting novel implications for both cosmology and astrophysics.

Although Rastall gravity introduces an unconventional mechanism, it has not escaped scrutiny. Visser [4] questioned its physical distinctiveness, suggesting it could be merely a reformulation of GR, while Golovnev [5] criticized the absence of a well-defined variational principle and cast doubt on its phenomenological utility. Despite such reservations, subsequent investigations have mounted compelling defenses of the theory. Darabi et al. [6], for instance, demonstrated its empirical adequacy in specific cosmological models, while others have constructed physically meaningful solutions that are not replicable within standard GR [7, 8]. This theory has also been affirmed in compact star modeling: Shahzad and Abbas employed the $\mathbb{MIT}$ bag model to examine strange stars [9], and later extended their work to include hybrid [10] and quintessence [11] stars. Naseer investigated the influence of the Rastall parameter on novel spherical solutions [12], and further explored the effects of gravitational decoupling in relation to isotropization and structural complexity [13]. His collaborative work with Sharif [14] involved the Krori-Barua and Tolman IV metrics within the context of decoupling and Rastall parameters. Other contributions include isotropic models derived using the Durgapal-Lake ansatz by Waseem and Naeem [15], and investigations by ourselves that generalized regular Hayward and Bardeen black holes [16]. Several promising results have emerged from various investigations into self-gravitating compact stars conducted within the context of this non-conserved gravity [17]-[24].

Gravitational decoupling, a method grounded in the application of geometric deformations - either in their minimal (MGD) or extended (EGD) form - has proven to be a robust framework for constructing novel solutions to the gravitational field equations. Within both GR and several modified gravity theories, this technique permits systematic generalizations through the separation of a known (commonly isotropic) solution from an auxiliary source term that produces direction-dependent behavior. The MGD and EGD schemes were both formulated by Ovalle [25, 26], where the minimal version involves deforming only g_{rr}, while the extended version modifies both g_{rr} and g_{tt}. These decoupling schemes have been instrumental in generalizing well-known solutions, such as the Tolman IV and Krori-Barua metrics, within GR and in the context of Brans-Dicke theory, to yield anisotropic models. Additionally, Ovalle and collaborators [27] employed this framework to derive hairy black hole solutions by extending the Schwarzschild vacuum geometry. The influence of the

Cite as: M. Sharif, M. Sallah, T. Naseer, East Eur. J. Phys. 3, 127 (2026), https://doi.org/10.26565/2312-4334-2026-3-11

2-step GD method has also been explored in the context of structural complexity [28]. In a recent investigation, Maurya et al. [29] applied the EGD scheme to extend the Tolman IV solution to a more complex domain and obtained a physical acceptable model.

In this study, we apply the EGD framework to deform the Schwarzschild black hole solution, subsequently linking it to a wormhole geometry. For detailed discussions on black hole deformations within this context, readers are referred to our earlier works [16, 29]. The theoretical origins of wormholes exist in the fundamental work of Misner and Wheeler [30, 31], who analyzed the creation of charge quantity from the continuity of field lines across discontinuities in spacetime. Wheeler [32, 33] was the first to propose "geons" and the concept of spacetime foam, thereby suggesting that the structure of spacetime becomes fundamentally intricate when examined at quantum-level resolutions. Even earlier, Einstein and Rosen had developed a geometric construct (now famously known as the Einstein-Rosen bridge [34]) which envisioned a throat-like structure connecting two asymptotically flat regions of spacetime. Although redolent of potential inter-universal passages, the viability of this configuration was subsequently contested by Fuller and Wheeler [35], who proved that the bridge is inherently unstable and undergoes collapse too rapidly to facilitate the traversal of either particles or light.

The resurgence of interest in wormhole physics can be traced largely to the seminal work of Morris and Thorne [36], who, through specific choices of redshift and shape functions, presented static, spherically symmetric, traversable wormhole solutions within the GR framework. A fundamental issue with these models, however, lies in their reliance on exotic matter - substances that violate the null energy conditions (NECs), thereby introduces deep theoretical complications. This challenge has sparked a shift towards exploring wormholes in the realm of modified gravity theories, where the violation of energy conditions can emerge from geometric modifications rather than physically implausible forms of matter. In such theories, effective EMTs can absorb the NECs violations through curvature-related contributions. As a result, wormhole solutions have been extensively studied in alternative frameworks like $f(\mathcal{R})$ gravity [37], Gauss-Bonnet gravity [38], and, significantly, in Rastall theory [39], where the usual conservation of the EMT is relaxed. This modification enables richer matter-geometry couplings that support wormhole structures without invoking exotic matter in the conventional sense. These developments not only offer plausible wormhole geometries but also deepen our understanding of how non-trivial topological configurations may naturally arise in extended theories of gravity.

The structure of the paper is given as follows. Section **2** is devoted to the formulation of the gravitational field equations within the Rastall gravity paradigm, thereby furnishing the theoretical groundwork to be used in the later analysis. In section **3**, the EGD formalism is used to split the field equations into decoupled sectors, making tractable solutions possible. Section **4** focuses on deriving a transformed static, spherically symmetric black hole solution and establishing its geometric link to a traversable wormhole configuration. This section also sets forth an extensive investigation of the wormhole derived, involving an inspection of NECs' violation, a calculation of active mass, an estimation of the volume integral quantifier ($\mathcal{VIQ}$), and a geometric illustration through an embedding schematic. Lastly, section **5** offers concluding remarks, highlighting the broader implications of our results for wormhole construction in the setting of modified gravity theories.

2. FIELD EQUATIONS

Within the context of the Rastall gravity, the equations dictating the dynamics adopt the following expression

$$G_{\mu\nu} = \kappa(T_{\mu\nu} - \xi\mathcal{R}g_{\mu\nu}). \tag{1}$$

Here, $G_{\mu\nu}$ is the Einstein tensor, $g_{\mu\nu}$ the metric tensor, $\mathcal{R}$ the Ricci scalar, κ the coupling constant, $T_{\mu\nu}$ the EMT, and the Rastall's coupling parameter $\lambda = \kappa\xi$. Within this approach, the EMT obeys the relationship given by

$$\nabla_\nu T^{\mu\nu} = \lambda g^{\mu\nu}\nabla_\nu\mathcal{R}, \tag{2}$$

which implies the usual covariant conservation law is violated. However, in the case where the λ parameter disappears, the ordinary conservation law of GR is once again obtained. From the relation in Eq.(1), it follows that

$$\mathcal{R}(4\lambda - 1) = \kappa T, \tag{3}$$

where T signifies the trace of the EMT $T_{\mu\nu}$. Finally, the governing equations of the spacetime geometry (1) may be written alternatively as

$$G_{\mu\nu} + \lambda\mathcal{R}g_{\mu\nu} = \frac{8\pi(1 - 4\lambda)}{1 - 6\lambda}T_{\mu\nu}. \tag{4}$$

Let us assume that $T_{\mu\nu}$ takes the form of an anisotropic fluid within the $(+, -, -, -)$ metric convention, written explicitly as

$$T_{\mu\nu} = (\rho + P_t)\mathcal{Y}_\mu\mathcal{Y}_\nu + (P_r - P_t)\mathcal{Z}_\mu\mathcal{Z}_\nu - P_t g_{\mu\nu}, \tag{5}$$

where

- $\mathcal{Y}_\mu = \delta^0_\mu\sqrt{g_{00}}$: 4-vector and $\mathcal{Z}_\mu = -\delta^0_\mu\sqrt{-g_{11}}$: four-velocity,
- ρ: density,

- P_r: radial pressure and P_t: transverse pressure.

Moreover, $\mathcal{Y}^\mu \mathcal{Y}_\mu = 1$, $\mathcal{Y}^\mu \mathcal{Z}_\mu = 0$ and $\mathcal{Z}^\mu \mathcal{Z}_\mu = -1$. To perform the gravitational decoupling technique, we alter the governing equations of the spacetime geometry (4) by employing a multi-sourced EMT, expressed in the following way as

$$G_{\mu\nu} + \lambda \mathcal{R} g_{\mu\nu} = \frac{8\pi(1-4\lambda)}{1-6\lambda} T_{\mu\nu}^{(tot)}, \tag{6}$$

where

$$T_{\mu\nu}^{(tot)} = T_{\mu\nu} + \delta \Psi_{\mu\nu}. \tag{7}$$

The incorporation of a supplementary source, denoted $\Psi_{\mu\nu}$, is achieved through the decoupling parameter δ, where δ dictates the magnitude of the coupling linking the sources. By introducing this term, anisotropic behavior emerges within the once-isotropic seed solution, which in turn expands its range of applicability to diverse contexts.

For the interior region, the geometric arrangement is provided by the following metric

$$ds^2 = -(d\theta^2 + \sin^2\theta d\phi^2) r^2 - e^{\mathcal{B}(r)} dr^2 + e^{\mathcal{A}(r)} dt^2. \tag{8}$$

After substitution, the field equations (6) are given by

$$\begin{aligned} 8\pi\left(\frac{4\lambda-1}{6\lambda-1}\right)\left(\rho + \delta\Psi_0^0\right) = \lambda\left[e^{-\mathcal{B}}\left(\mathcal{A}'' + \frac{\mathcal{A}'}{2}(\mathcal{A}'-\mathcal{B}') + \frac{2}{r}(\mathcal{A}'-\mathcal{B}') + \frac{2}{r^2}\right) - \frac{2}{r^2}\right] \\ + e^{-\mathcal{B}}\left(\frac{\mathcal{B}'}{r} - \frac{1}{r^2}\right) + \frac{1}{r^2}, \end{aligned} \tag{9}$$

$$\begin{aligned} 8\pi\left(\frac{4\lambda-1}{6\lambda-1}\right)\left(P_r - \delta\Psi_1^1\right) = -\lambda\left[e^{-\mathcal{B}}\left(\mathcal{A}'' + \frac{\mathcal{A}'}{2}(\mathcal{A}'-\mathcal{B}') + \frac{2}{r}(\mathcal{A}'-\mathcal{B}') + \frac{2}{r^2}\right) - \frac{2}{r^2}\right] \\ + e^{-\mathcal{B}}\left(\frac{\mathcal{A}'}{r} + \frac{1}{r^2}\right) - \frac{1}{r^2}, \end{aligned} \tag{10}$$

$$\begin{aligned} 8\pi\left(\frac{4\lambda-1}{6\lambda-1}\right)\left(P_t - \delta\Psi_2^2\right) = -\lambda\left[e^{-\mathcal{B}}\left(\mathcal{A}'' + \frac{\mathcal{A}'}{2}(\mathcal{A}'-\mathcal{B}') + \frac{2}{r}(\mathcal{A}'-\mathcal{B}') + \frac{2}{r^2}\right) - \frac{2}{r^2}\right] \\ + e^{-\mathcal{B}}\left[\frac{\mathcal{A}''}{2} + \frac{\mathcal{A}'^2}{4} - \frac{\mathcal{A}'\mathcal{B}'}{4} + \frac{\mathcal{A}'-\mathcal{B}'}{2r}\right]. \end{aligned} \tag{11}$$

There are three nonlinear ordinary differential equations in the above system, expressed in terms of $\mathcal{A}, \mathcal{B}, \rho, P_r, P_t, \Psi_0^0, \Psi_1^1, \Psi_2^2$, where the prime notation means $' = \frac{d}{dr}$. With the help of this system, we formulate the effective variables in the following manner

$$\tilde{\rho} = \rho + \delta\Psi_0^0, \quad \tilde{P}_r = P_r - \delta\Psi_1^1, \quad \tilde{P}_t = P_t - \delta\Psi_2^2, \tag{12}$$

and anisotropic parameter

$$\tilde{\Delta} = \tilde{P}_t - \tilde{P}_r = \delta(\Psi_1^1 - \Psi_2^2). \tag{13}$$

The condition $\Psi_1^1 = \Psi_2^2$ implies the absence of anisotropy in the additional source, indicating that the anisotropic factor vanishes. In the subsequent section, we apply the EGD method to address the field equations (9)-(11). This technique facilitates the decomposition of the full system into two distinct subsystems: one associated with the original (seed) EMT $T_{\mu\nu}$, and the other corresponding to the supplementary source $\Psi_{\mu\nu}$. Owing to the reduced coupling, each sector can be treated and solved independently. The full solution to the field equations is then constructed through a linear superposition of these individual solutions, as prescribed in Eq.(12).

3. AN EGD APPROACH

To address the system of equations (9)-(11), we adopt the EGD approach, which introduces linear deformations to both g_{rr} and g_{tt}. Through these deformations, the original system is effectively decoupled into two distinct sectors. The first corresponds to a perfect fluid configuration (achieved by setting $\delta = 0$), while the second incorporates the effects of the additional source $\Psi_{\mu\nu}$, expressed in terms of the deformation functions. As a starting point, we consider a well-established ideal fluid solution to the field equations, characterized by the following metric

$$ds^2 = -(d\theta^2 + \sin^2\theta d\phi^2) r^2 - \frac{dr^2}{\mathcal{D}(r)} + e^{\mathcal{C}(r)} dt^2, \tag{14}$$

with
$$\mathcal{D}(r) = 1 - \frac{2m(r)}{r}, \tag{15}$$
where m represents the Misner-Sharp mass. The linear transformations that characterize the geometric deformation are given by
$$C(r) \mapsto \mathcal{A}(r) = C(r) + \delta f(r), \quad \mathcal{D}(r) \mapsto e^{-\mathcal{B}(r)} = \mathcal{D}(r) + \delta g(r), \tag{16}$$
where $f(r)$ and $g(r)$ denote the deformations applied to the g_{tt} and g_{rr}, respectively. Substituting Eq.(16) into the field equations produces the first set given below
$$8\pi\left(\frac{1-4\lambda}{1-6\lambda}\right)\rho = \mathcal{D}\left(\lambda C'' + \frac{\lambda C'^2}{2} + \frac{2\lambda C'}{r} + \frac{2\lambda}{r^2} - \frac{1}{r^2}\right) - \frac{2\lambda}{r^2} + \frac{1}{r^2} + \mathcal{D}'\left(\frac{\lambda C'}{2} + \frac{2\lambda}{r} - \frac{1}{r}\right), \tag{17}$$
$$8\pi\left(\frac{1-4\lambda}{1-6\lambda}\right)P_r = \mathcal{D}\left(\frac{C'}{r} + \frac{1}{r^2} - \frac{2\lambda}{r^2} - \frac{2\lambda C'}{r} - \frac{\lambda C'^2}{2} - \lambda C''\right) + \frac{2\lambda}{r^2} - \frac{1}{r^2} - \mathcal{D}'\left(\frac{\lambda C'}{2} + \frac{2\lambda}{r}\right), \tag{18}$$
$$8\pi\left(\frac{1-4\lambda}{1-6\lambda}\right)P_t = \mathcal{D}\left(\frac{C''}{2} - \lambda C'' - \frac{\lambda C'^2}{2} - \frac{2\lambda C'}{r} - \frac{2\lambda}{r^2} + \frac{C'^2}{4} + \frac{C'}{2r}\right) + \frac{2\lambda}{r^2} + \mathcal{D}'\left(\frac{C'}{4} + \frac{1}{2r} - \frac{\lambda C'}{2} - \frac{2\lambda}{r}\right). \tag{19}$$
Since the system consists of three linearly independent equations involving five unknowns: $C, \mathcal{D}, \rho, P_r$, and P_t, two additional constraints are required to render it solvable. In the following section, we impose these constraints by invoking the vacuum Schwarzschild solution as the guiding framework.

The second set of equations, which separates the contribution from the supplemental source and the deformation function, may be expressed as
$$8\pi\left(\frac{1-4\lambda}{1-6\lambda}\right)\Psi_0^0 = \lambda\left[g\left(C'' + \frac{(C')^2}{2} + \frac{2C'}{r}\right) + g'\left(\frac{C'}{2} + \frac{2}{r}\right) + \mathcal{D}f'' + \mathcal{D}C'f' + \frac{\mathcal{D}\delta(f')^2}{2} + \frac{\mathcal{D}'f'}{2} + \frac{2\mathcal{D}f'}{r}\right] - \frac{g'}{r} - \frac{g}{r^2}, \tag{20}$$
$$8\pi\left(\frac{1-4\lambda}{1-6\lambda}\right)\Psi_1^1 = \lambda\left[g\left(C'' + \frac{(C')^2}{2} + \frac{2C'}{r}\right) + g'\left(\frac{C'}{2} + \frac{2}{r}\right) + \mathcal{D}f'' + \mathcal{D}C'f' + \frac{\mathcal{D}\delta(f')^2}{2} + \frac{\mathcal{D}'f'}{2} + \frac{2\mathcal{D}f'}{r}\right] - g\left(\frac{C'}{r} + \frac{1}{r^2}\right) - \frac{\mathcal{D}f'}{r}, \tag{21}$$
$$8\pi\left(\frac{1-4\lambda}{1-6\lambda}\right)\Psi_2^2 = \lambda\left[g\left(C'' + \frac{(C')^2}{2} + \frac{2C'}{r}\right) + g'\left(\frac{C'}{2} + \frac{2}{r}\right) + \mathcal{D}f'' + \mathcal{D}C'f' + \frac{\mathcal{D}\delta(f')^2}{2} + \frac{\mathcal{D}'f'}{2} + \frac{2\mathcal{D}f'}{r}\right] - g\left(\frac{C''}{2} + \frac{(C')^2}{4} + \frac{C'}{2r}\right) - \frac{\mathcal{D}'f'}{4} - g'\left(\frac{C'}{4} + \frac{1}{2r}\right) - \mathcal{D}\left(\frac{f''}{2} + \frac{\delta(f')^2}{4} + \frac{\mathcal{D}'f'}{2} + \frac{f'}{2r}\right). \tag{22}$$
To solve the system of equations (20)-(22), we impose two supplementary constraints, given that it contains five unknowns but only three independent equations. To be more precise, we adopt both a linear $\mathbb{E}\text{o}\mathbb{S}$ and a mimic constraint expressed in terms of the total pressure. The equation sets (17)-(19) and (20)-(22) provide a decoupled representation of the primary field equations (9)-(11), and the full solution to the original system can be recovered by linearly adding the solutions obtained from each.

4. FROM BLACK HOLE TO WORMHOLE MODELS

This portion of the work explores the development of a wormhole model connected to a totally distorted black hole of the non-Schwarzschild sort. Considering the Schwarzschild spacetime

$$ds^2 = \left(1 - \frac{2M}{r}\right) dt^2 - \frac{dr^2}{\left(1 - \frac{2M}{r}\right)} - r^2 d\Omega^2, \tag{23}$$

the EGD scheme described in the previous section deforms this metric to

$$ds^2 = \left(1 - \frac{2M}{r}\right) e^{\delta f(r)} dt^2 - \frac{dr^2}{\left(1 - \frac{2M}{r} + \delta g(r)\right)} - r^2 d\Omega^2. \tag{24}$$

Clearly, the deformed spacetime depicted the above configuration differs from Schwarzschild geometry in that $|g_{tt}(r)| \neq |g_{rr}^{-1}(r)|$. It thus represents a non-Schwarzschild black hole. Our objective is to generate a wormhole geometry in association with the present spacetime. To do this however, we must first of all determine the deformation functions $f(r)$ and $g(r)$ in order to completely represent the deformed spacetime above. We obtain these deformation functions by employing two constraints in the system of equations (20)-(22). For the first of these constraints, we employ a linear $\mathbb{E}\mathrm{o}\mathbb{S}$ on $\Psi_{\mu\nu}$ given as

$$\Psi_0^0 - \zeta_1 \Psi_1^1 - \zeta_2 \Psi_2^2 = 0, \tag{25}$$

where ζ_1 and ζ_2 are real constants. By setting $\zeta_1 = 1$ and $\zeta_2 = 0$, we obtain the simplified form given by

$$\Psi_0^0 = \Psi_1^1. \tag{26}$$

Using Eqs.(20) and (21), this equation turns out to

$$f'(r) = \frac{g'(r) - g(r)C'(r)}{\mathcal{D}(r)}. \tag{27}$$

For the second constraint, we adopt the total pressure mimic-constraint given by

$$\frac{1}{3}\left(P_r + 2P_t\right) = \frac{1}{3}\left(\Psi_1^1(r) + 2\Psi_2^2(r)\right). \tag{28}$$

However, since $P_r = P_t = 0$ due to the vacuum seed solution, this equation reduces to

$$\Psi_1^1(r) + 2\Psi_2^2(r) = 0. \tag{29}$$

Using Eq.(27) in this constraint, we deduce numerical solutions for the deformations which are plotted in **Figure 1**. It is important to emphasize that our objective here is not to analyze the physical characteristics of the black hole spacetime itself, but rather to construct a wormhole geometry that is geometrically connected to it. For a detailed treatment of the extended gravitational decoupling of the Schwarzschild black hole, we refer readers to our earlier work [29]. In the discussion that follows, we focus on identifying the conditions under which the spacetime described by Eq.(24) can be interpreted as a viable wormhole solution.

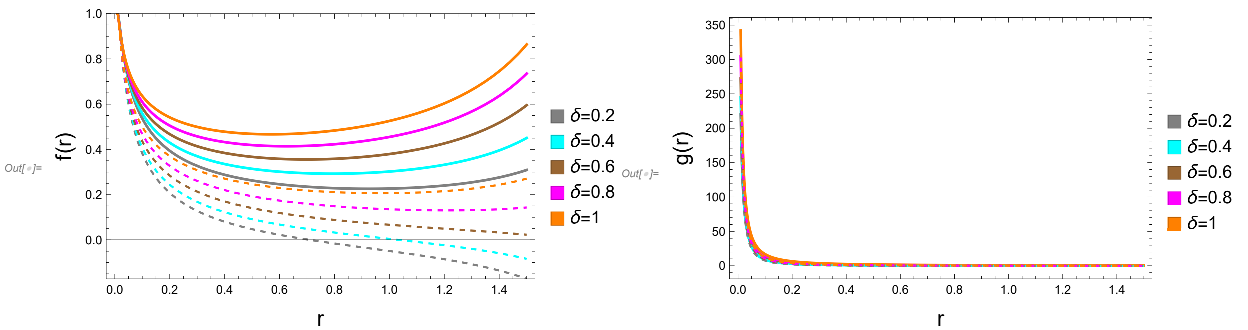

Figure 1. Deformation functions $f(r)$ and $g(r)$.

4.1. A Wormhole Solution

The Morris-Thorne metric, representing the most general spacetime, is adopted for the description of the wormhole geometry [36]

$$ds^2 = e^{2\eta(r)}dt^2 - \frac{dr^2}{1-\frac{\chi(r)}{r}} - r^2 d\Omega^2. \tag{30}$$

Here, the wormhole structure is described by the shape function $\chi(r)$, and $\eta(r)$ plays the role of the redshift function. Relating this spacetime interval to the one from Eq.(24) gives the direct consequence that

$$\eta(r) = \frac{1}{2}\left(\delta f(r) + \ln\left|1-\frac{2M}{r}\right|\right), \tag{31}$$

and

$$\chi(r) = 2M - \delta r g(r). \tag{32}$$

The wormhole throat (r_0) is obtained from the relation $\chi(r_0) = r$. However, an explicit form of the wormhole throat cannot be given as the deformation function $g(t)$ is numerically approximated. To reinforce the validity of the proposed wormhole model, we examine several essential geometric conditions, illustrated in **Figure 2**. Among these, the flare-out condition plays a central role. Mathematically, it is expressed as

$$\frac{\chi(r) - r\chi'(r)}{2\chi^2(r)} > 0, \tag{33}$$

such a condition ensures the throat takes the shape of a minimal surface that expands outward, a key prerequisite for keeping the throat stable and ensuring it can be crossed. This condition provides an essential bridge between wormhole geometry and the requirement for exotic matter, marking it as a foundational concept in wormhole physics. Moreover, we demonstrate how the shape function $\chi(r)$ behaves under the condition $\chi(r) < r$, applicable for every r. We also confirm asymptotic flatness by plotting $\chi(r)/r$ and demonstrating its vanishing behavior at large radial distances. In each of the pertinent plots, we use representative choices of the Rastall parameter as $\lambda = 0.175$ (solid) and $\lambda = 0.225$ (dashed). The decoupling parameter δ takes specific values for each figure, and these are indicated alongside wherever applicable.

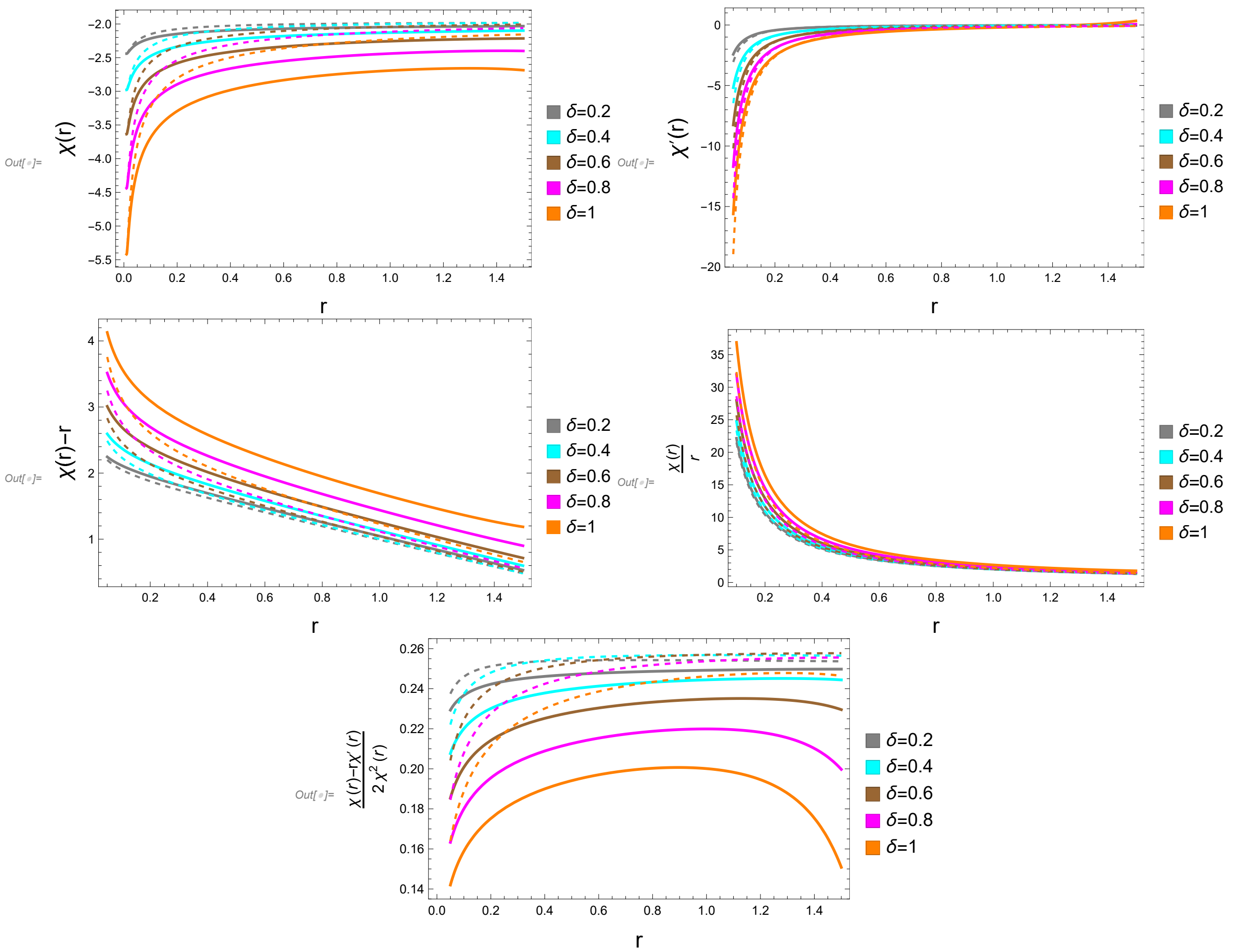

Figure 2. Some geometric properties with $\lambda = 0.175$ (solid) and 0.225 (dashed).

4.2. Energy Conditions

Energy conditions represent foundational constraints in theoretical physics, governing the permissible distributions of energy and momentum throughout spacetime. A complete appreciation of these conditions is indispensable for exploring the sophisticated interactions occurring between geometry and matter. The universe consists of numerous energy forms, including baryonic matter, dark matter, exotic matter, and dark energy, all of which respond in context-dependent ways to the physical conditions around them. Identifying suitable geometric frameworks capable of accommodating such varied forms of energy remains a central and ongoing challenge in modern gravitational theory.

The analysis of traversable wormholes becomes significantly more complicated, given that their production involves transgressing the usual energy condition framework. These requirements are customarily separated into four basic categories, which are the null, weak, dominant, and strong conditions. The occurrence of non-standard matter is generally accompanied by the violation of these conditions. Among them, the NECs are particularly critical, as their violation often entails the breakdown of the remaining three. For this reason, our investigation into the viability and physical properties of the wormhole solution focuses primarily on the behavior of the NECs, expressed as

$$\tilde{\rho} + \tilde{P}_r \geq 0, \quad \tilde{\rho} + \tilde{P}_t \geq 0.$$

These inequalities are evaluated and illustrated in **Figure 3**, where the plots clearly indicate that the NECs are violated, thus confirming the presence of exotic matter required to sustain the wormhole geometry.

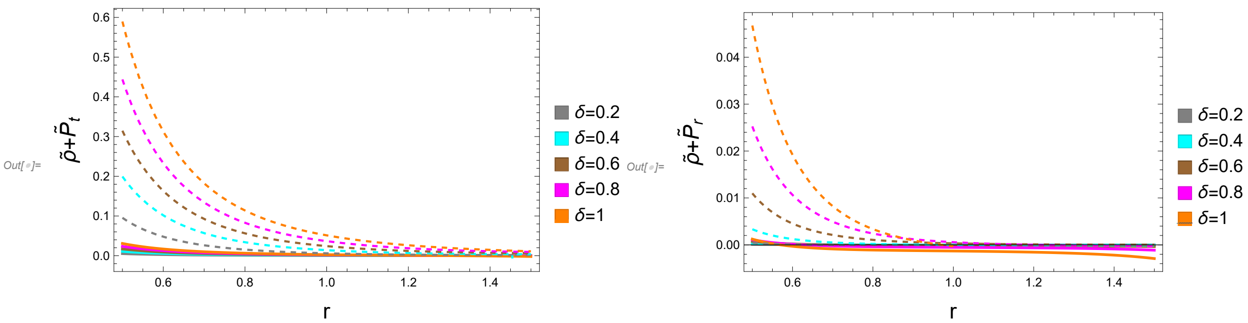

Figure 3. NECs with $\lambda = 0.175$ (solid) and 0.225 (dashed).

4.3. Embedding Diagram

An embedding diagram offers a visual representation of the spatial curvature around a wormhole by depicting a lower-dimensional spatial slice embedded in a higher-dimensional Euclidean space. Although wormholes exist in four-dimensional spacetime, these diagrams simplify the geometry-typically by focusing on an equatorial, constant-time surface-to illustrate key features such as the flaring at the throat, which geometrically manifests the throat expansion condition.

The construction of this diagram takes as its point of departure the Morris-Thorne metric given by Eq.(30). To examine the geometric properties of space, we adopt a static equatorial slice defined by t = constant and $\theta = \frac{\pi}{2}$; this procedure results in the following two-dimensional spatial line element

$$ds^2 = \frac{dr^2}{1 - \frac{\eta(r)}{r}} + r^2 d\phi^2. \tag{34}$$

We target the embedding of this two-dimensional surface visualized within flat three-dimensional Euclidean geometry parameterized by cylindrical coordinates (r, ϕ, z), for which the metric can be expressed as

$$ds^2 = \left[1 + \left(\frac{dZ}{dr}\right)^2\right] dr^2 + r^2 d\phi^2. \tag{35}$$

Comparing Eq.(34) with (35) above, we obtain

$$\frac{dZ}{dr} = \pm\sqrt{\frac{\chi(r)}{r - \chi(r)}}. \tag{36}$$

Setting Eq.(34) equal to (35) allows us to obtain the differential equation governing the embedding surface $Z(r)$ as

$$\frac{dZ}{dr} = \pm\sqrt{\frac{\chi(r)}{r - \chi(r)}}. \tag{37}$$

This relation defines how the spatial geometry of the wormhole can be embedded in a higher-dimensional Euclidean space. **Figure 4** demonstrates the resulting embedding diagram, where the horizontal axis corresponds to the radial coordinate. The graph shows how each $Z(r)$ curve distinguishes between the higher ($Z(r) > 0$) and lower ($Z(r) < 0$) portions of space, creating a clear geometric representation of the wormhole's anatomy. Consistent with the flaring-out condition for traversability, the figure shows the throat as the narrowest point and the surrounding geometry expanding outward with larger r. Consistent with the flaring-out condition for traversability, the figure shows the throat serving as the constriction point and the surrounding geometry expanding outward with larger r.

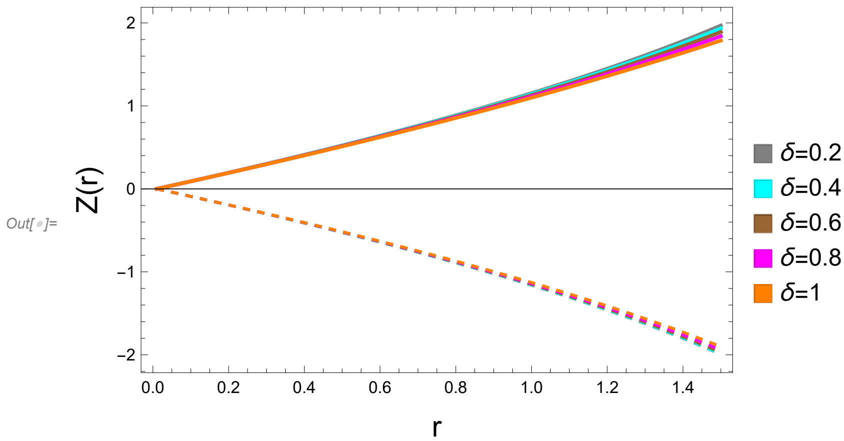

Figure 4. Embedding diagram with $\lambda = 0.175$ (solid) and 0.225 (dashed).

4.4. Gravitational Mass

This section is devoted to analyzing the effective gravitational mass associated with the wormhole configuration, particularly in the context of dark matter-supported geometries. We compute the mass across the wormhole's spatial region, which runs from the neck radius r_0 to an unspecified radial coordinate r, using the integral expression provided by [40]

$$M_G = 4\pi \int_{r_0}^{r} \tilde{\rho}\, r^2\, dr, \tag{38}$$

that we assess through numerical evaluation. The results indicate that the mass accumulates more rapidly in the vicinity of the throat, underscoring the throat's dominant influence on the wormhole gravitational characteristics. This quantity of effective mass is essential for calculating the gravitational environment that nearby material objects encounter. Our investigation prioritizes the active gravitational mass obtained from the wormhole geometry, which is presented in **Figure 5**. A discernible trend emerges from the figure: the active mass commences at a relatively elevated value and steadily falls off with increasing radial coordinate. Interestingly, it becomes negative near the wormhole mouth, signaling the presence of exotic matter in that region. Such a negative mass behavior is a strong indication of energy condition violations, further supporting the physical plausibility of Passable wormholes within the present theoretical framework.

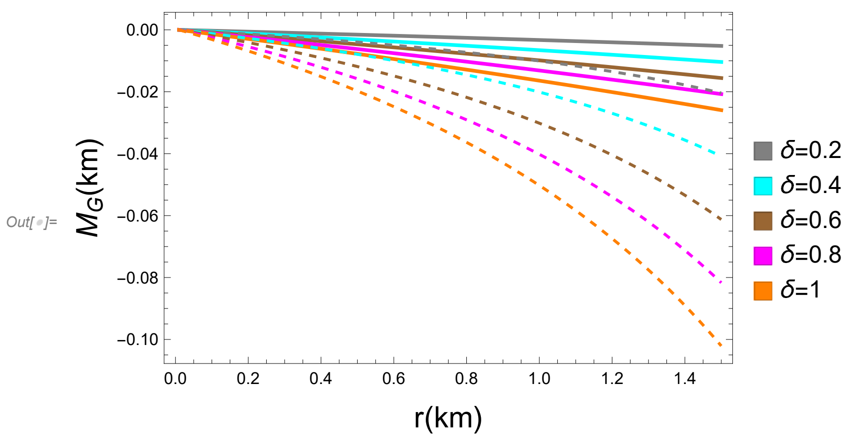

Figure 5. Gravitational mass for $\lambda = 0.175$ (solid) and 0.225 (dashed).

4.5. Volume Integral Quantifier

The $\mathcal{VIQ}$ functions as a helpful diagnostic in wormhole theory, specifically designed to calculate the aggregate exotic matter necessary for maintaining a traversable wormhole. This method, originally presented by Visser and colleagues [41], evaluates the potential to minimize any violation of the NECs. Specifically, the $\mathcal{VIQ}$ assesses the total integrated presence of matter violating the null energy condition by carrying out a spatial volume integral across the relevant parts of the EMT, given as

$$\mathcal{VIQ} = \int (\tilde{\rho} + \tilde{P}r)dV = 8\pi \int_{r_0}^{\infty} (\tilde{\rho} + \tilde{P}_r)r^2 dr. \tag{39}$$

This integral is assessed through numerical technique, and its values are presented in **Figure 6**. A negative value for $\mathcal{VIQ}$ substantiates the existence of exotic matter inside the wormhole's interior. Notably, the magnitude of this exotic matter decreases sharply near the throat, indicating that only a small quantity is necessary in that region to maintain the wormhole's structure. This result suggests that, with an appropriately chosen geometric profile, the total requirement for exotic matter can be significantly reduced.

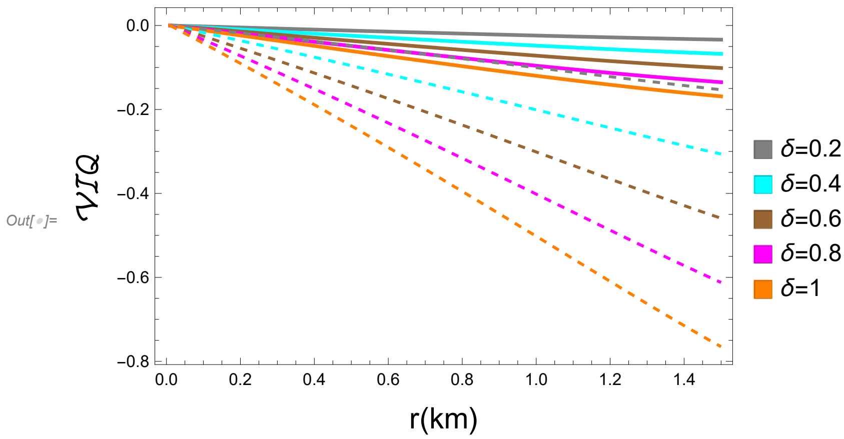

Figure 6. $\mathcal{VIQ}$ for $\lambda = 0.175$ (solid) and 0.225 (dashed).

5. CONCLUSIONS

This investigation reports a traversable wormhole solution constructed in Rastall gravity through the application of the EGD approach to the Schwarzschild black hole. We began our study using the updated Rastall field equations and, using the EGD technique, inserted a supplemental gravitational source that keeps all metric components altered. This led to a black hole solution that is minimally deformed, which was then smoothly converted into a wormhole spacetime by appropriately matching it to the Morris-Thorne expression. Our wormhole metric maintained asymptotic flatness while displaying a well-defined throat, its position and behavior were derived from the collective contribution of the mass function, the δ parameter, and the λ parameter. The redshift function stayed limited and singularity-free, verifying the lack of event horizons and confirming that the solution allows traversal. A detailed geometric study revealed that the flare-out requirement is perfectly satisfied at the throat, demonstrating that the wormhole structure is physically feasible.

To substantiate the viability of the model, we have conducted a comprehensive investigation of several physical and geometric indicators. We investigated the NECs using the effective EMT and discovered that they were violated close to the neck across all parameter configurations, indicating the manifestation of exotic material. Nonetheless, the violation is localized in space and becomes progressively smaller at larger values of r. We clearly visualized the wormhole structure and its two asymptotically flat regions through the geometric representation provided by the embedding diagram. We have furthermore investigated the gravitational mass, which demonstrates a diminishing trend and attains negativity in the throat region, an additional fingerprint of exotic matter. Additionally, we have evaluated the $\mathcal{VIQ}$ to estimate the total amount of NECs-violating matter. Our numerical outcomes suggest that the exotic matter necessarily can be kept quite small when the Rastall and decoupling parameters are chosen appropriately. Overall, our analysis demonstrates that Rastall gravity, when supplemented via the EGD technique, gives an appealing avenue for generating physically plausible wormholes, thereby decreasing the theoretical obstacles that have hampered their acceptance. Future investigations may explore extensions to dynamical or rotating wormhole geometries, as well as stability analysis under linear or nonlinear perturbations.

Data Availability Statement: No data was used for the work described in this research.

ORCID

Muhammad Sharif, https://orcid.org/0000-0001-6845-3506; **Malick Sallah**, https://orcid.org/0009-0007-9677-6653; **Tayyab Naseer**, https://orcid.org/0000-0002-9436-810X

REFERENCES

[1] S. Capozzielo, E. De-Filippis, and V. Salzano, Mon. Not. R. Astron. Soc. **394**, 947 (2009). https://doi.org/10.1111/j.1365-2966.2008.14382.x

[2] A.V. Astashenok, S. Capoziello, M.D. Laurentis, and S.D. Odinstov, J. Cosmol. Astropart. Phys. **01**, 001 (2015). https://doi.org/10.1088/1475-7516/2015/01/001

[3] P. Rastall, Phys. Rev. D, **6**, 3357 (1972). https://doi.org/10.1103/physrevd.6.3357

[4] M. Visser, Phys. Lett. B, **782**, 83 (2018). https://doi.org/10.1016/j.physletb.2018.05.028

[5] A. Golovnev, Ann. Phys. **461**, 169580 (2024). https://doi.org/10.1016/j.aop.2023.169580

[6] F. Darabi, H. Moradpour, I. Licata, Y. Heydarzade, and C. Corda, Eur. Phys. J. C, **78**, 25 (2018). https://doi.org/10.1140/epjc/s10052-017-5502-5

[7] F. Darabi, K. Atazadeh, and Y. Heydarzade, Eur. Phys. J. Plus, **133**, 249 (2018). https://doi.org/10.1140/epjp/i2018-12083-1

[8] S. Hansraj, A. Banerjee, and P. Channuie, Ann. Phys. **400**, 320 (2019). https://doi.org/10.1016/j.aop.2018.12.003

[9] M.R. Shahzad, and G. Abbas, Int. J. Geom. Methods Mod. Phys. **16**, 1950132 (2019). https://doi.org/10.1142/s0219887819501329

[10] M.R. Shahzad, and G. Abbas, Astrophys. Space Sci. **365**, 147 (2020). https://doi.org/10.1007/s10509-020-03861-y

[11] M.R. Shahzad, and G. Abbas, Eur. Phys. J. Plus, **135**, 1 (2020). https://doi.org/10.1140/epjp/s13360-020-00508-3

[12] T. Naseer, Phys. Dark Universe, **46**, 101663 (2024). https://doi.org/10.1016/j.dark.2024.101663

[13] T. Naseer, Eur. Phys. J. C, **84**, 1256 (2024). https://doi.org/10.1140/epjc/s10052-024-13634-4

[14] T. Naseer, and M. Sharif, Class. Quantum Grav. **41**, 245006 (2024). https://doi.org/10.1088/1361-6382/ad8d9d

[15] A. Waseem, and S. Naeem, Phys. Scr. **99**, 125023 (2024). https://doi.org/10.1088/1402-4896/ad8e92

[16] M. Sharif, and M. Sallah, Chin. J. Phys. **92**, 794 (2024). https://doi.org/10.1016/j.cjph.2024.09.027

[17] C.E. Mota, L.C.N. Santos, G. Grams, F.M. da Silva, and D.P. Menezes, Phys. Rev. D, **100**, 024043 (2019). https://doi.org/10.1103/PhysRevD.100.024043

[18] P. Bhar, F. Tello-Ortiz, Á. Rincón, and Y. Gomez-Leyton, Astrophys. Space Sci. **365**, 145 (2020). https://doi.org/10.1007/s10509-020-03859-6

[19] G. Mustafa, and T.C. Xia, Int. J. Mod. Phys. A, **35**, 2050109 (2020). https://doi.org/10.1142/s0217751x20501092

[20] M. Zubair, S. Waheed, M.F. Jamal, and G. Mustafa, Results Phys. **29**, 104787 (2021). https://doi.org/10.1016/j.rinp.2021.104787

[21] C.E. Mota, L.C.N. Santos, F.M. da Silva, G. Grams, I. P. Lobo, and D.P. Menezes: Int. J. Mod. Phys. D, **31**(4), 2250023 (2022). https://doi.org/10.1142/S0218271822500237

[22] G.G.L. Nashed, Universe, **8**, 510 (2022). https://doi.org/10.3390/universe8100510

[23] A. Ashraf, M.R. Shahzad, Z. Zhang, E. Güdekli, and M.F. Jamal, Phys. Scr. **98**, 035027 (2023). https://doi.org/10.1088/1402-4896/acb6bd

[24] W. El Hanafy, and A. Awad, Astrophys. J., **951**, 144 (2023). https://doi.org/10.3847/1538-4357/acd93c

[25] J. Ovalle, Phys. Rev. D, **95**, 104019 (2017). https://doi.org/10.1103/physrevd.95.104019

[26] J. Ovalle, Phys. Lett. B, **788**, 213 (2019). https://doi.org/10.1016/j.physletb.2018.11.029

[27] J. Ovalle, R. Casadio, E. Contreras, and A. Sotomayor, Phys. Dark Universe, **31**, 100744 (2021). https://doi.org/10.1016/j.dark.2020.100744

[28] C.L. Heras, and P. Leon, Gen. Relativ. Gravit. **54**, 138 (2022). https://doi.org/10.1007/s10714-022-03031-1

[29] S.K. Maurya, K.N. Singh, and B. Dayanandan, Eur. Phys. J. C, **80**, 448 (2020). https://doi.org/10.1140/epjc/s10052-020-8005-8

[30] C.W. Misner, and J.A. Wheeler, Ann. Phys. **2**, 525 (1957). https://doi.org/10.1016/0003-4916(57)90049-0

[31] C.W. Misner, Phys. Rev. **118**, 1110 (1960). https://doi.org/10.1103/physrev.118.1110

[32] J.A. Wheeler, Ann. Phys. **2**, 604 (1957). https://doi.org/10.1016/0003-4916(57)90050-7

[33] J.A. Wheeler, Int. J. Mod. Phys. A, **3**, 2207 (1988). https://doi.org/10.1142/s0217751x88000941

[34] A. Einstein, and N. Rosen, Phys. Rev. **48**, 73 (1935). https://doi.org/10.1103/physrev.48.73

[35] R.W. Fuller, and J.A. Wheeler, Phys. Rev. **128**, 919 (1962). https://doi.org/10.1103/physrev.128.919

[36] M.S. Morris, and K.S. Thorne, Am. J. Phys. **56**, 395 (1988). https://doi.org/10.1119/1.15620

[37] F.S.N. Lobo, and M.A. Oliveira, Phys. Rev. D, **80**, 104012 (2009). https://doi.org/10.1103/physreva.80.012112

[38] M. R. Mehdizadeh, M. K. Zangeneh, and F. S. N. Lobo, Phys. Rev. D, **91**, 084004 (2015). https://doi.org/10.1103/physrevd.91.084004

[39] H. Moradpour, N. Sadeghnezhad, and S.H. Hendi, Can. J. Phys. **95**, 1257 (2017). https://doi.org/10.1139/cjp-2017-0040

[40] C.W. Misner, and D.H. Sharp, Phys. Rev. **136**, B571 (1964). https://doi.org/10.1103/physrev.136.b571

[41] M. Visser, S. Kar, and N. Dadhich, Phys. Rev. Lett. **90**, 201102 (2003). https://doi.org/10.1103/physrevlett.90.201102

РІШЕННЯ ДЛЯ ПРОХОДНИХ ЧЕРВОТОЧКОВИХ РІШЕНЬ ЗА ДОПОМОГОЮ ПІДХОДУ РОЗДІЛУ В ТЕОРІЇ РАСТАЛЛА

Мухаммад Шаріф[1,2], **Малік Саллах**[1], **Тайяб Насір**[1]
[1]*Кафедра математики та статистики, Лахорський університет, 1-KM Defence Road Lahore-54000, Пакистан*
[2]*Дослідницький центр Джадара, Університет Джадара, Ірбід 21110, Йорданія*

У цій статті досліджується побудова рішень прохідних червоточин у контексті гравітації Расталла з використанням розширеного методу гравітаційного розв'язання. На основі модифікованих польових рівнянь цієї нової теорії ми застосовуємо цю схему для включення додаткового гравітаційного джерела, що призводить до повністю перетвореної версії рішення Шварцшильда. За допомогою відповідного перетворення координат ця модифікована геометрія переосмислюється як простір-час червоточини. Аналіз продовжується дослідженням фундаментальних фізичних та геометричних характеристик результуючої конфігурації, зокрема, порушення умов нульової енергії, поведінки гравітаційної маси, оцінки квантора об'ємного інтеграла та діаграми вбудовування. Ключовим висновком є те, що шийка червоточини очевидно виникає внаслідок спотвореної геометрії, водночас задовольняючи критерій розширення, необхідний для прохідності. Побудова графіків енергетичних умов для різних значень параметрів Расталла виявляє локалізовані порушення умов нульової енергії поблизу шийки, що узгоджується з наявністю екзотичної матерії. Однак, показано, що загальний вміст екзотичної матерії є мінімальним та дуже чутливим до вибору параметрів моделі. Ці результати підкреслюють потенціал гравітації Расталла, у поєднанні з гравітаційним роз'єднанням, для підтримки фізично правдоподібних геометрій червоточин зі зменшеними вимогами до екзотичної матерії.

Ключові слова: *теорія Расталла; гравітаційне роз'єднання; червоточини; екзотична рідина*